J. Fluid Mech. (1975), *vol.* 71, *part* 3, *pp.* 541–562
Printed in Great Britain

Mean and turbulence characteristics of three-dimensional wall jets

By N. V. CHANDRASEKHARA SWAMY AND P. BANDYOPADHYAY†

Fluid Mechanics Laboratory, Department of Applied Mechanics, Indian Institute of Technology, Madras 36

(Received 8 April 1974 and in revised form 25 April 1975)

This paper reports experimental investigations on the characteristic decay and the radial-type decay regions of a three-dimensional isothermal turbulent wall jet in quiescent surroundings. The velocity and the length scale behaviour for both the longitudinal and the transverse directions are studied, and compared with the results of other workers. The estimated skin friction is discussed in relation to the available data from earlier investigations. Wall jet expansion rates and the behaviour of skin friction are also discussed. The rate of approach of turbulence components to a self-similar form is found to be influenced by the fact that the expansion rate of the wall jet in the longitudinal direction is different from that in the transverse.

1. Introduction

In the recent past, considerable research effort has been devoted to a class of flows which can be recognized as a combination of free and wall turbulent shear flows. These flows are called *wall jets* or *wall wakes*. They not only have a very wide practical application, but are also interesting in themselves, as an example of interaction between free-jet and boundary-layer types of flow.

Glauert (1956) analysed the problem of a turbulent wall jet by dividing the flow regime into two parts: the region between the wall and the point of maximum velocity as a normal boundary layer, called the *inner layer*; and the rest of the wall jet with the features of a free jet, called the *outer layer*. He matched the solutions for the two layers at the point of maximum velocity, where the shear stress was assumed to be zero. Glauert also showed that similarity of the complete velocity profile is not possible for a turbulent wall jet. This was reflected in the different exponents for maximum velocity decay and spread rate in the two layers.

Since Glauert's pioneering work, a great deal of attention has been devoted to the study of plane and radial wall jets, and extensive literature is available today. However, in practice, such two-dimensional geometries are rarely encountered. Three-dimensional wall jets, which occur more often in practical situations, have started receiving attention only in recent years.

† Present address: Engineering Laboratory, University of Cambridge.

The earliest work reported on three-dimensional wall jets is an experimental study of Viets & Sforza (1966), who described the mean flow characteristics in the region of flow establishment. The flow was generated by employing rectangular orifices of various aspect ratios (height/length). Three-dimensionality of the flow arises owing to finiteness and squareness of the orifice. An important finding reported by Sforza & Herbst (1970) is that the centre-line maximum velocity decay occurs in three stages. The first stage is the *potential core* (PC) region, where the maximum velocity in the wall jet is constant. This is followed by the second stage, called the *characteristic decay* (CD) region, where the decay exponent is dependent on the orifice geometry. Lastly, the decay follows the pattern for axisymmetric wall jets (i.e. the flow becomes oblivious of the orifice geometry from which it originated). This is called the *radial-type decay* (RD) region. Clearly, similarity in the velocity profiles is possible only in this last region, since the flow is then independent of the conditions at its origin.

Newman *et al.* (1972) investigated the three-dimensional wall jet originating from a circular orifice. In this work, variation of the velocity and length scales was predicted by neglecting wall friction, and assuming an approximate similarity condition to exist in the far downstream region. Measurements of mean velocity and longitudinal turbulence showed good agreement between measured and predicted values of the scales.

In spite of the differences existing in the structure of turbulence between boundary layers and wall jets (Bandyopadhyay 1974), the mean velocity profile of the inner layer of the wall jet exhibits some features of two-dimensional turbulent boundary-layer profiles. By analogy, one can expect a behaviour in the inner layer of a three-dimensional wall jet similar to that in a three-dimensional turbulent boundary layer. This is borne out by the recent experiments of Chandrasekhara Swamy & Lakshmana Gowda (1974). The wall jet was generated by means of one-half of a round nozzle (similar to the present case) and measurements were confined to distances very close to the jet (12 radii in the longitudinal direction). Different secondary flow models were tested in that work, and some mean characteristics of the wall jet in the PC and CD regions determined.

Very little information seems to be available about the turbulence characteristics of three-dimensional wall jets, however. Also, from a practical point of view, the region of the wall jet close to the orifice is more important than that far downstream. But the flow here is more complex, because of the existence of several different flow regimes and an appreciable pressure gradient near the orifice. For these reasons, an investigation was carried out on the flow field of a three-dimensional incompressible isothermal wall jet in the region close to the orifice including the PC, CD and the beginning of the RD regions. The wall jet was generated by the tangential flow of air from one-half of a round nozzle on to a smooth flat plate in an otherwise stagnant surrounding. The details of the experimental facility are given in § 2. The mean flow characteristics are discussed in § 3; and § 4 presents results concerning the turbulence quantities.

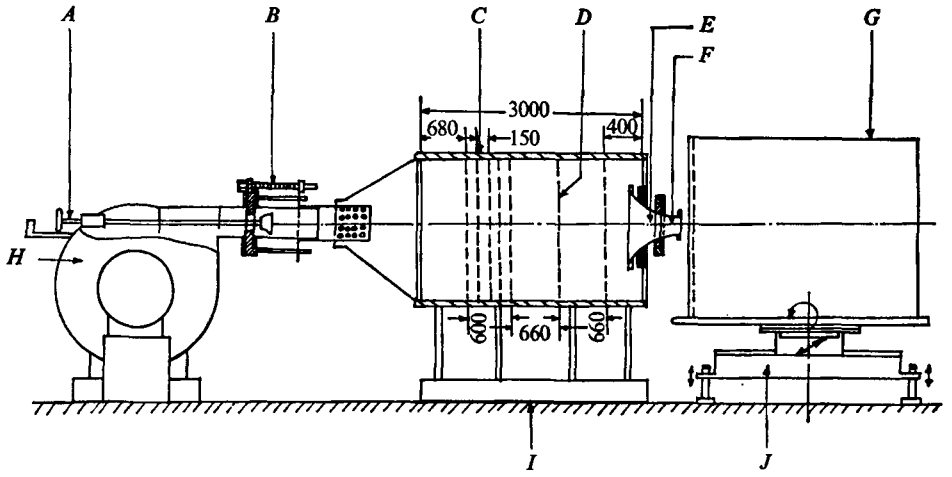

FIGURE 1. Schematic of apparatus. Not to scale. *A*, throttle control; *B*, bypass control; *C*, settling chamber; *D*, screens (30 mesh); *E*, nozzle (100 mm dia.); *F*, nozzle (57 mm dia.); *G*, flat plate; *H*, centrifugal blower; *I*, vibration isolation; *J*, plate support.

2. Experimental procedure

The experimental facility is essentially the same as that used in Chandrasekhara Swamy & Lakshmana Gowda. Figure 1 shows a sketch of the wind tunnel with the model. Air is supplied from a centrifugal blower, driven by a 15 kW motor. The supply of air is controlled by a throttle placed in the inlet section (velocity variation is less than 0·2 mm water column in a 4 h run). The air stream is led into a settling chamber through a symmetrical diffuser. The settling chamber is 3 m long with a cross-section 1 × 1 m. This is supported on a concrete foundation, which is isolated from the laboratory floor. The chamber is provided with 8 nylon screens of fine mesh, to straighten the flow and to reduce turbulence. The chamber is fitted with an aluminium nozzle of 100 mm dia. at the exit end. For the present studies, a 57 mm dia. nozzle made of aluminium was screwed onto the 100 mm nozzle, to avoid spilling of the wall jet over the sides of the flat plate. This also allowed measurements to be made up to a distance of 40 radii. Though the smoothness of the nozzle at the interface was apparently not disturbed, it was felt necessary to conduct a preliminary study of the 57 mm dia. free jet. This study showed that the flow field characteristics of the jet corresponded to those of standard free jets.

It was felt necessary in the present set-up to find out if the surroundings were truly quiescent. This is important, because Hanjalić & Launder (1972) doubted whether this condition is satisfied in usual wall jet experiments. Since the present study was confined to the region close to the nozzle exit (i.e. within 1·2 m from the nozzle), the 1 × 1 m frontage provided by the settling chamber near the nozzle could be considered sufficient to prevent any draught in the laboratory from that direction. In addition, the flat plate, on which the wall jet was generated, also inhibited the room draught, if any, from affecting the quiescent surroundings condition. Corrsin (1943), in his free jet studies, found that the fully developed

region of the jet up to 40 dia. was not affected by the presence or absence of a wall near the nozzle. Hence, the present experimental arrangement can be considered to be quite satisfactory. Also, enclosing the flow field in screen cages was deemed unnecessary, since the region of interest was quite close to the nozzle.

Initially, a flat plate 1·2 m long, 0·92 m wide and 28 mm thick (made of 17 plywood laminations, glued together in orthotropic fashion) was used to produce the wall jet. Preliminary tuft tests showed spillage of the wall jet in the spanwise directions. Subsequently, two teak-wood flats, each 1·2 m long, 0·25 m wide and 26 mm thick, were fitted to the two sides of the plate, to make a wider plate of length 1·2m and width 1·42 m. This was found to be adequate, by tuft tests and subsequent spanwise velocity profile measurements. The plate surface was smoothed, and a visual check by a thin stainless-steel standard flat, before and at the end of the experiments (a few months later), indicated no warping of the combined piece of plate. Static pressure measurements on the plate also showed negligible waviness of the surface.

The plate was fixed vertically to an apparatus having three degrees of freedom, to facilitate easy alignment. The leading edge was chamfered to 45° (to avoid pressure-gradient effects due to a rounded leading edge), and was placed at a distance of 22 mm from the nozzle face. Since the plate was placed in the diametral plane and within the potential core of the free jet (which extended up to 8 radii), the initial gap was assumed to have no effect on the wall jet development (cf. Sridhar & Tu 1966). Probe movement was accomplished with the help of a traversing mechanism. A simple optical arrangement was used first to align the traversing mechanism with respect to the nozzle. Subsequently, the plate was positioned with the help of the traversing mechanism. Sample spanwise velocity profile measurements showed the flow to be symmetrical about the centre-line within experimental accuracy. This was further supported by a few $\widetilde{u'w'}$ measurements, which were found to be practically zero. Displacements of the probe larger than 1 mm, and away from the wall, were measured by scales fixed to the traversing mechanism. Near-wall measurements were made using dial gauges mounted on magnetic bases. Most of the experiments were performed with a nozzle exit velocity of approximately 20 m s^{-1}.

The inner layer of the near-flow field of the present wall jet was found to be three-dimensional in nature (cf. Chandrasekhara Swamy & Lakshmana Gowda). Also, since the present study was confined to the flow field near the nozzle exit, it was necessary to know the axial wall static pressure distribution. For these reasons, the model was provided with static pressure taps both in the longitudinal and the spanwise directions. The tap positions are shown in figure 2, which also contains an inset of the static pressure taps used. It can be seen, from this figure, that these taps have been fixed at distances of $(2nR + 5)$ mm from the leading edge (where R is the nozzle radius and n varies from 1 to 20). Since all velocity measurements were made at distances of $2nR$ from the leading edge, the static pressure taps were provided 5 mm behind these points, so as not to interfere with the velocity measurements, especially very close to the wall. Sufficient care was taken in preparing these pressure taps so that optically magnified (× 100) views of the holes were clean and circular. Corrections to static pressure measurements

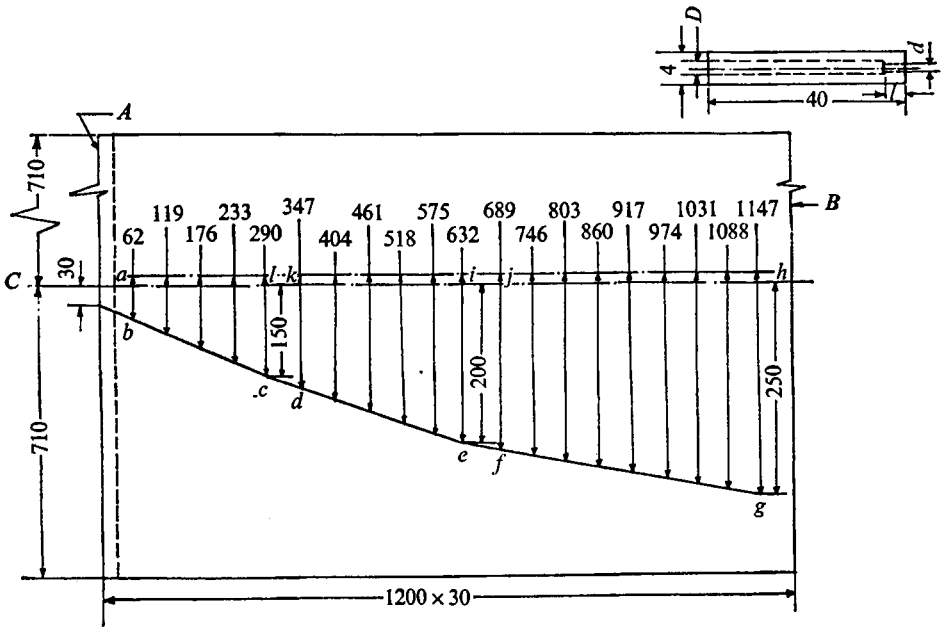

FIGURE 2. Pressure tap locations on flat plate. Pressure tap pitch: region *abcla*, pitch = 8; *kdeik*, 10; *jfghj*, 15. Dimensions in mm; not to scale. *A*, knife edge (45°); *B*, distance from knife edge where pressure taps are located; *C*, nozzle centre-line. Inset: $d = 0{\cdot}3$ dia.; $l = 3$; $D = 1{\cdot}5$.

were estimated by the procedure due to Shaw (1960), and were found to be negligibly small.

Mean and turbulence velocity measurements in the wall jet were performed by DISA 55A22 hot-wire probes made of 1·2 mm long Pt-plated tungsten wire of 5 μm dia. The probe was connected to a DISA 55D01 anemometer operated in constant temperature mode. The d.c. and a.c. components of the signal were measured by DISA 55D30 Digital d.c. and DISA 55A35 r.m.s. voltmeters respectively. To avoid inaccuracies due to drift, the probes were calibrated after every run of approximately 3 h.

The $\tilde{u}'$ turbulence component was measured mainly by the single-wire technique. A cross-wire technique, due to Lawn (1969), was used to measure the $\tilde{v}'$ and $\tilde{w}'$ turbulence components. For this purpose, the leads of a miniature X-probe (DISA 55A38) were connected to two DISA 55D01 anemometers, both operating in constant-temperature mode. Both signals were then linearized by two DISA 55D15 linearizers. The sensitivities of the wires were matched by connecting a DISA 55D25 amplifier to one of the linearized signals. Instantaneous values of the matched signals were then added, subtracted and squared by a DISA 55D70 correlator.

Corrections to the mean velocity readings due to turbulence, calculated according to Hinze (1959), were of the order of 8 % in the inner layer. But towards the outer edge of the outer layer, this correction reached a value as high as 15 %. It is known (Lawn 1969) that, though for mean velocity measurements any value of the calibration exponent between 0·45 and 0·5 can be used, Reynolds stress

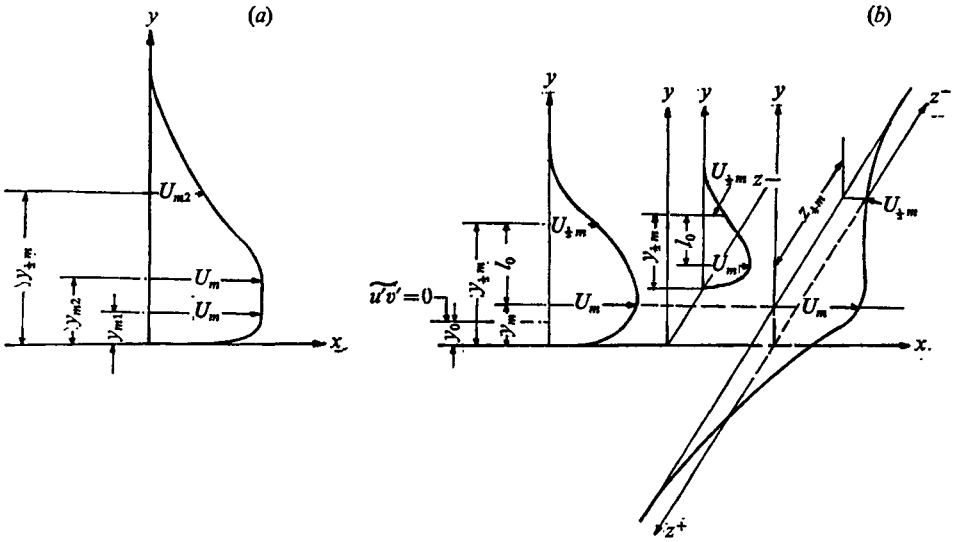

FIGURE 3. Definition sketches of velocity profiles. (*a*) PC region; (*b*) CD and RD regions, x axis = nozzle centre-line.

evaluation will be in gross error if an exponent of 0·5 is used. Hence a value of 0·45 was used in all the mean velocity and longitudinal turbulence calculations.

A definition sketch for the velocity and length scales for the PC, CD and RD regions for the present case is given in figure 3.

3. Mean flow characteristics of the wall jet

3.1. *Wall static pressure variation: longitudinal and spanwise*

The wall static pressure distribution was measured both in the longitudinal and along one of the spanwise directions at a nozzle exit velocity of 20 m s^{-1}. Since the flow was symmetrical about the centre-line, measurement in the spanwise direction was deemed necessary only on one side of the centre-line. The distribution along the centre-line was also measured at a flow velocity of 30 m s^{-1}.

The centre-line wall static pressure variation is shown in figure 4 (*a*) for both the velocities. The static pressure is everywhere much smaller in magnitude than the jet dynamic head. There is a large variation in the region close to the jet exit, however. The high positive pressure rapidly drops to zero, and assumes a negative value, though smaller in magnitude. The figure also shows little dependence of the pressure on the velocities considered, which is a check on the reproducibility of the measurements.

Figure 4 (*b*) shows the spanwise variation of wall static pressure at two x-wise stations. It can be seen from the figures 4 (*a*) and (*b*) that, except for a small region, approximately covering a little more than the potential core, the wall static pressure is everywhere nearly atmospheric.

3.2. *Velocity and length scales*

The gross characteristics of free shear flows are normally described by the rate of decay of maximum velocity and the spread rate. The relevant characteristics

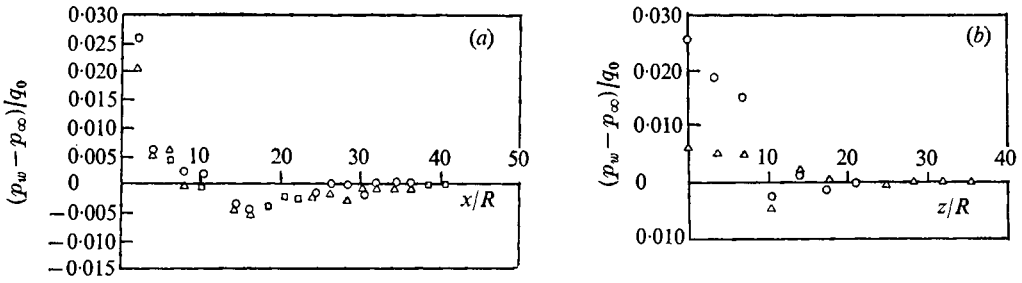

FIGURE 4. Wall static pressure p_w variation. (*a*) Centre-line at $U_j = 20$ (○) and 30 m s^{-1} (△). (*b*) Spanwise at $x = 32$ (○) and 11 mm (△). Atmospheric pressure p_∞; jet exit dynamic head q_0.

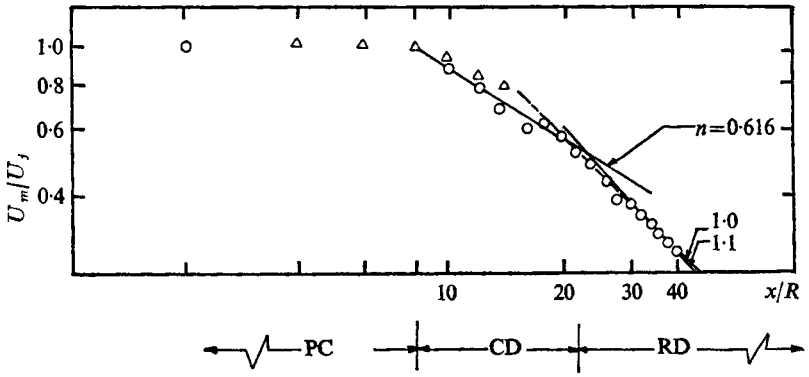

FIGURE 5. Decay of maximum velocity in the plane of symmetry of the wall jet. △, Chandrasekhara Swamy & Lakshmana Gowda.

for a three-dimensional wall jet are the maximum velocity decay and spread rates of the inner and the outer layers in the plane of symmetry, as well as the length scale l_0, defined in figure 3.

Figure 5 shows the maximum velocity decay in the plane of symmetry. Normally, in free shear flows, maximum velocity decay is expressed by a power law, viz.

$$U_m/U_j \propto (x/R)^{-n},$$

where U_m is the maximum velocity for any x and U_j is the jet efflux velocity. An exponent of 0·62 describes the decay between $x/R = 10$ and 20 quite well. Beyond this, the exponent changes to 1·1, which is typical of radial-type decay (Poreh, Tsuei & Cermak 1967). Following Sforza & Herbst (1970), the flow field here can also be divided into three distinct regimes, depending upon the decay rate of maximum velocity.

The velocity profiles exhibit a region of constant maximum velocity approximately up to $x/R = 8$. This is the potential core region. Between $x/R = 10$ and 20, the decay follows a pattern which is neither two-dimensional nor radial. Since Sforza & Herbst did not notice any monotonic trend in n with eccentricity, a comparison between different values of n cannot be made conclusively. It can only be mentioned here that $n = 0{\cdot}62$ is close to the two-dimensional values of 0·5

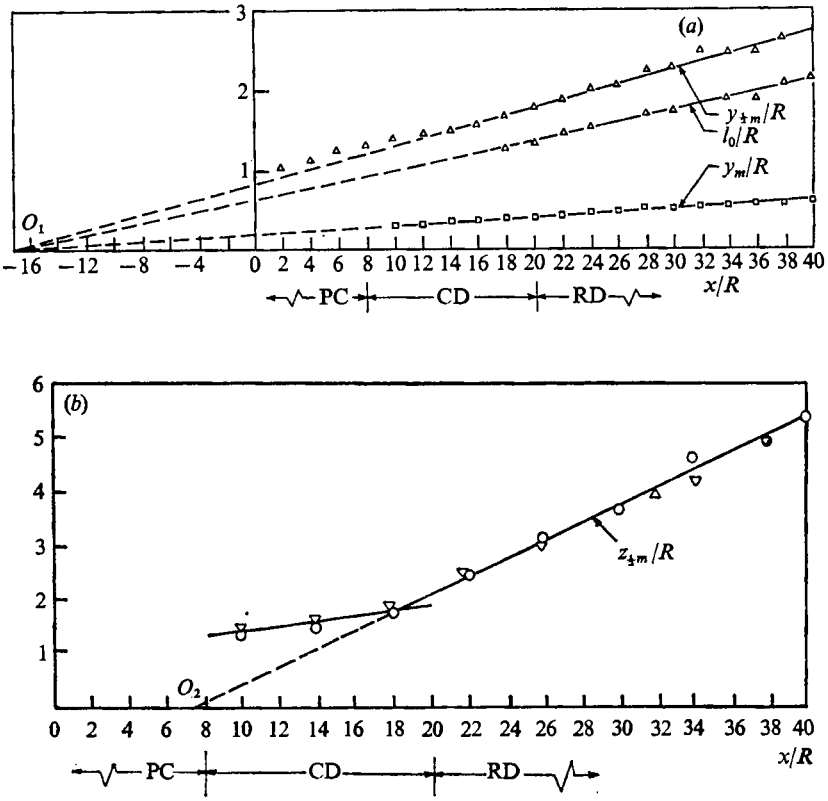

FIGURE 6. Growth of length scales (*a*) in the plane of symmetry ($\frac{1}{2}y_m$, l_0, y_m), (*b*) in the lateral plane through $\frac{1}{2}z_m$. ○, $+z$ direction; △, $-z$ direction.

(Sigalla 1958) and 0·55 (Schwarz & Cosart 1961). It can also be noted that, in the CD region, Sforza & Herbst (1970) and Patankar & Sridhar (1972) (the latter called it CDI region) obtained values of n that were lower than those in the two-dimensional case, whereas they are higher in the present case.

Next to the CD region (i.e. $x/R > 22$), the rate of decay is faster than that of the radial type. A line with $n = 1$ is also shown in figure 5. This is the value obtained by Newman *et al.* from dimensional arguments; and it was verified by them experimentally. At axial distances beyond $x/R = 20$, this trend is followed closely here, indicating a faster rate of flow development

The longitudinal variation of the length scales y_m, $y_{\frac{1}{2}m}$ and l_0 is shown in figure 6 (*a*). In the RD region, all length scales vary linearly with x/R, a situation similar to that observed by Newman *et al.*, lending support to their similarity analysis. These scales indicate a virtual origin at $x/R = -17{\cdot}5$ for the flow in the RD region and in the plane of symmetry. In Newman *et al.*'s case, the virtual origin was located at $x/D = -19$.

The spread rate of the spanwise flow can be represented by the variation of the corresponding length scale, $z_{\frac{1}{2}m}$, along the axial direction. This is shown in figure 6 (*b*). The spread of the spanwise flow is seen to be about 3·5 times greater than that normal to the plate in the plane of symmetry. The spread rates in the

region beyond $x/R = 18$ (i.e. towards the end of the CD region and the beginning of the RD region) are given by

$$\frac{dl_0}{dx} = 0{\cdot}046 \quad \text{and} \quad \frac{dz_{\frac{1}{2}m}}{dx} = 0{\cdot}166.$$

The corresponding values in the case of Newman *et al.* are 0·042 and 0·278 respectively. Therefore, though the growth rate in the plane of symmetry normal to the plate is nearly the same for both cases, the spanwise growth is 1·7 times greater in the case of Newman *et al.*

The spanwise spread of the flow in the CD region for the present wall jet contrasts strongly with the case of rectangular orifices of Sforza & Herbst (1970), especially for eccentricities smaller than unity. In the latter case, the flow does not seem to show a tendency to spread in the spanwise direction in the CD region. This conclusion may be drawn from the result of Sforza & Herbst that the spanwise half-length remains constant, and in some cases even reduces in the CD region for all eccentricities smaller than unity. This can be attributed to the strong horseshoe vortices which are generated by the sharp corners of the rectangular orifices. Sforza & Herbst noted that these vortices cause velocity irregularities, which are smoothed out before the RD region commences. The flow in the CD region is, obviously, affected by these irregularities, and it is likely that they slow down the velocity decay process and the rate of spread in the spanwise direction. Such irregularities were not observed in the present case, as shown by measurements of spanwise velocity profiles downstream of $x/R = 10$.

On the basis of the present results and those of Newman *et al.*, it may be concluded that a spread greater in the spanwise than in the normal direction is characteristic of three-dimensional wall jets.

It is seen from figure 6 (*b*) that the variation of $z_{\frac{1}{2}m}$ with x is monotonic, unlike the case of rectangular orifices. Beyond $x/R = 18$, the spread rate increases, and follows a linear trend, as required by the similarity condition of Newman *et al.*'s analysis. This happens approximately in the RD region. This spread rate indicates a virtual origin at $x/R = +7$. It can be recalled that the flow in the plane of symmetry had indicated a virtual origin at $x/R = -17{\cdot}5$. This occurrence of two virtual origins, far from each other, seems to be peculiar to three-dimensional wall jets, which has also been observed by Newman *et al.* However, in their cases, the virtual origins were at $x/D = +17$ and -19, much farther apart than in our case.

3.3. *Mean velocity profiles*

The mean flow development of the wall jet for the present geometry in the region of the potential core was described in detail in Chandrasekhara Swamy & Lakshmana Gowda. Hence, in the present discussion, only the similarity forms of the velocity profiles will be discussed.

The first similarity in the mean velocity profile is exhibited in the outer region in the plane of symmetry ($z = 0$) and within the PC region. The flow here can be considered to be that due to a simple annular free shear layer. The non-dimensional velocity profiles are shown in figure 7 for $x/R = 2$, 4 and 6. In this figure, the usual free shear co-ordinates are used, with x' denoting the longitudinal distance from

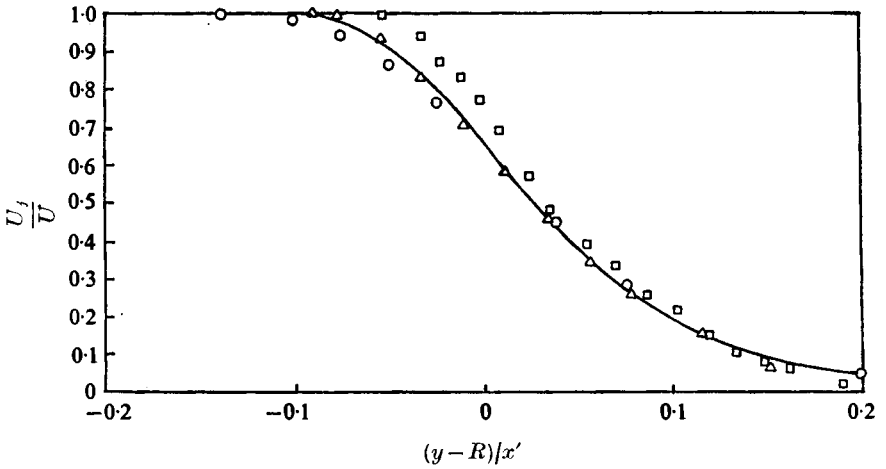

FIGURE 7. Wall-jet mixing-layer mean velocity profiles at $x/R = 2$ (○), 4 (△) and 6 (□). ——, Davies *et al.*

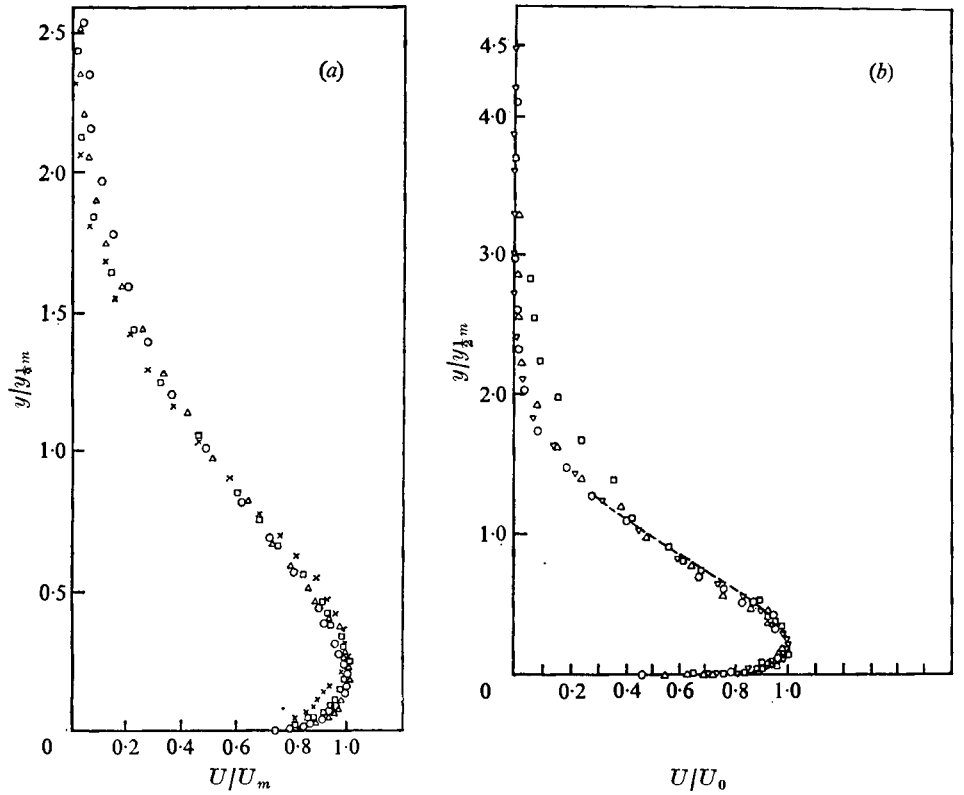

FIGURE 8. Similarity of velocity profiles (*a*) in the plane of symmetry of the wall jet, (*b*) in the lateral planes at $x/R = 20$. - - -, Glauert, $\alpha = 1{\cdot}3$.

(*a*) x/R	×	□	△	○
	10	20	30	40
(*b*) z/R	▽	○	△	□
	0	0·7	1·4	2·45

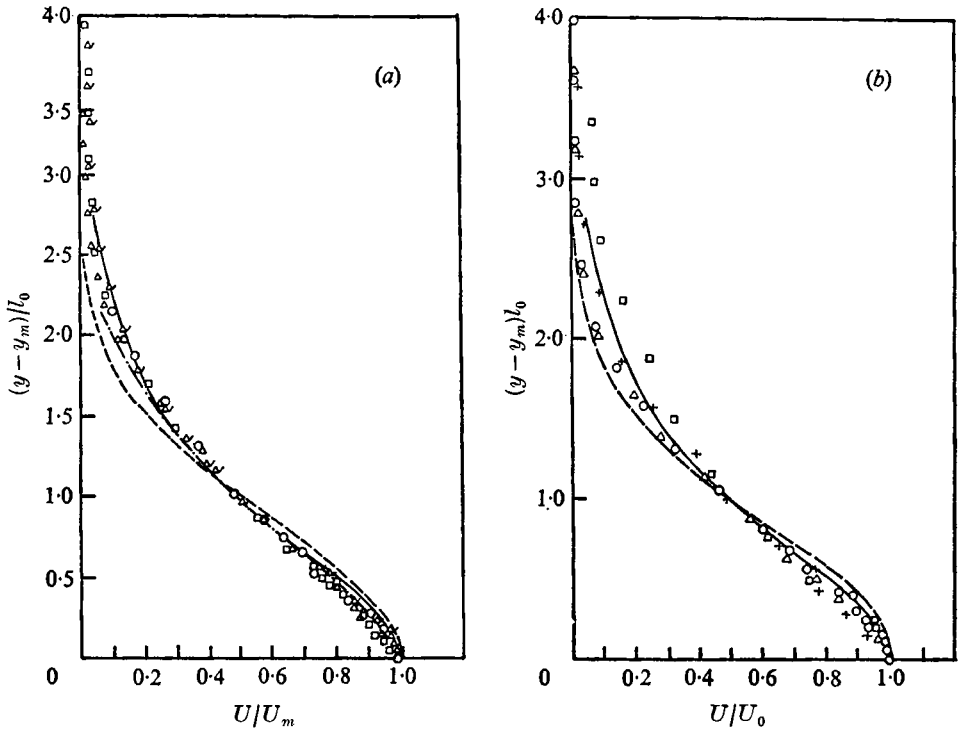

FIGURE 9. Similarity of the mean velocity profiles in the outer layer of the wall jet (*a*) in the plane of symmetry in the RD region, (*b*) in the lateral planes at $x/R = 20$. ——, axisymmetric free jet solution; - - -, Newman *et al.*, $U/U_m = \exp[-\ln 2\,\{(y-y_m)/l_0\}^2]$; — · — · —, Schwartz & Cosart, 2DWJ in still air.

(*a*) x/R	△	□	○	△
	30	34	36	38
(*b*) z/R	○	△	+	□
	0	0·7	1·4	2·45

the orifice mouth (i.e. $x' = x + 22\,\text{mm}$). For comparison, the measured mean velocity profile in the mixing zone of a round free jet, due to Davies, Fisher & Barratt (1963), is also given in the figure. It is seen that the agreement between the two sets of data is quite good.

The complete wall jet profiles, at $x/R = 10$, 20, 30 and 40 and in the plane of symmetry, are shown in figure 8 (*a*). The velocities are normalized by the maximum velocity at the location and the lengths by $y_{\frac{1}{2}m}$ (figure 3). Except at $x/R = 10$, the profiles are seen to have achieved a good similarity form. Profile similarity can be assumed to exist from $x/R = 20$ onwards. However, Newman *et al.* observed similarity in mean velocity profiles only beyond $x/D = 20$. In this context, it should be remembered that the present wall jet was generated by half a round nozzle, whereas the wall jet of Newman *et al.* was generated by keeping the orifice flush with the plate. This might cause some difference in flow development, though at larger distances, both cases can be expected to reach the same similar form. Keeping this in mind, it can be concluded at this stage only that the velocity profiles have reached a similar form in the region

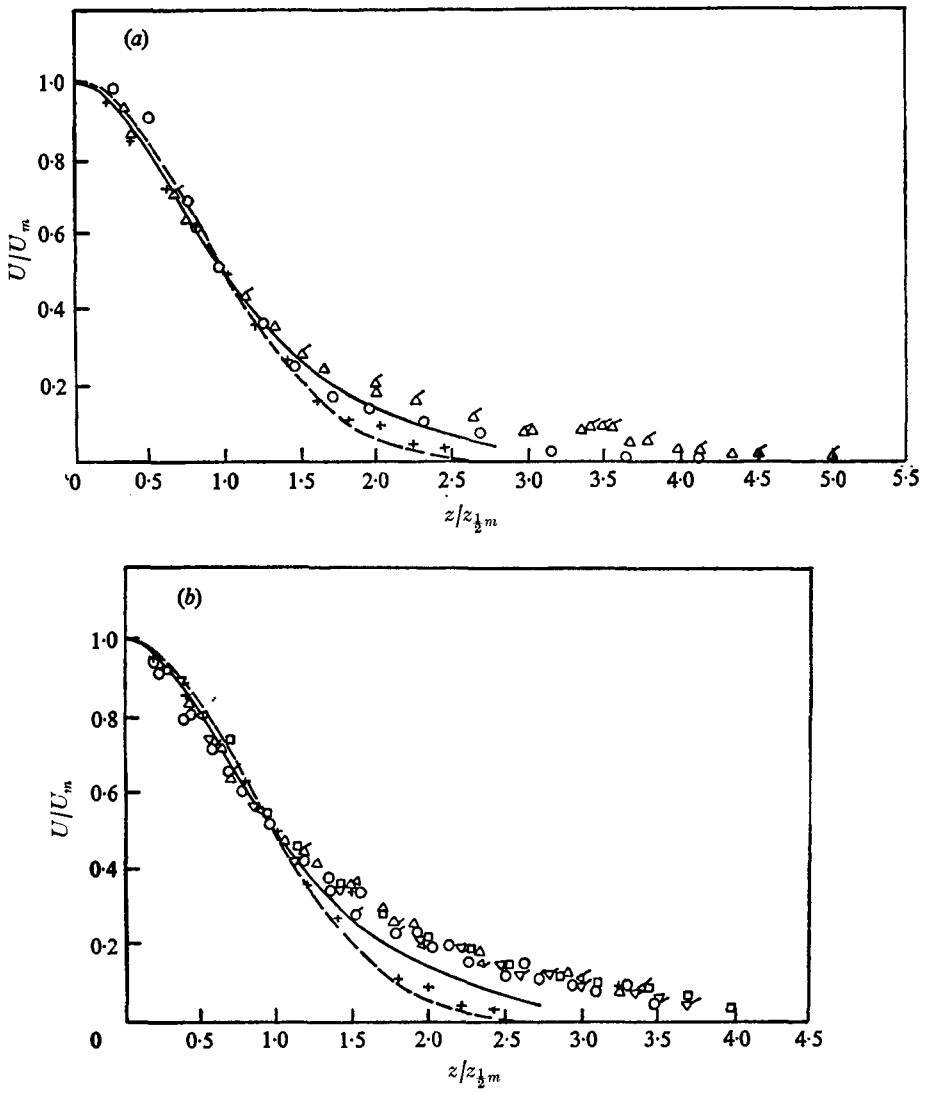

FIGURE 10. Similarity of the lateral velocity profiles at $y = y_m$ in (*a*) CD region and (*b*) RD region of the wall jet, together with free jet measurement at $17D$ from the nozzle face. ——, axisymmetric free jet solution; - - -, exponential profile.

(*a*) x/R	○	△	◁			
	10	14	18			
(*b*)	○	△	◯	□	◁	▽
	40	38	34	30	26	22

considered, but may still be undergoing a small change before they reach their final form in the later stages of the RD region.

The longitudinal velocity profiles, measured at lateral positions $z/R = 0{\cdot}7$, $1{\cdot}4$ and $2{\cdot}45$, and at $x/R = 20$, are shown in figure 8 (*b*) along with the profile for the plane of symmetry ($z = 0$) for the same x/R. Glauert's solution for radial wall jets with $\alpha = 1{\cdot}3$ is also shown, for comparison. It is seen that Glauert's

solution represents the data well up to $y = y_{\frac{1}{2}m}$, beyond which the scatter in the measured data is rather high.

Figure 9 (*a*) shows the velocity profiles of the outer layer in the plane of symmetry and in the RD region, plotted in a non-dimensional form suggested by Newman *et al.* The exponential profile due to Newman *et al.*,

$$\frac{U}{U_m} = \exp\left[-\ln 2\left(\frac{y-y_m}{l_0}\right)^2\right],$$

is also included. The free jet profile, as given by Schlichting (1968), is also shown for comparison. It is seen that Schlichting's profile gives better agreement with the data than the above expression. A poor agreement with the exponential profile has also been reported in Chandrasekhara Swamy & Lakshmana Gowda at $x/R = 14$, which was taken to imply that the profile was still undergoing a change. The difference between Newman *et al.*'s data, which agreed well with the exponential profile, and the present may be due to the different rates of flow development. Schwarz & Cosart's (1961) two-dimensional wall jet profile, with which Newman *et al.*'s measurements agree very well, is also shown in figure 9 (*a*). It may be seen that there is good agreement with our measurements, indicating that the velocity profile around $x/R = 40$ has already reached the form obtained by Newman *et al.* for $x/D = 50$. Further evidence for this is the fact that Newman *et al.*'s spread rate and maximum velocity decay exponent for the RD region are here reached around $x/R = 40$.

The longitudinal velocity profiles in the outer layer for the lateral positions as in figure 8 (*b*) are shown in figure 9 (*b*), along with the profile for the plane of symmetry. Similarity exists among the profiles in the lateral planes, but deteriorates beyond $z/R = 1{\cdot}4$. The exponential and the free jet profiles are also shown for comparison. The latter seems to describe the data better than the former.

Mean velocity profiles were measured in the spanwise direction, on both sides of the centre-line, at a distance from the wall where maximum velocity occurs in the plane of symmetry. The results for one spanwise direction are given in figure 10 (*a*) for the CD region and in figure 10 (*b*) for the RD region. The velocity and length scales are those shown in figure 3. Similarity of the velocity profiles may be seen to exist in both the regions. The figures also contain the exponential and free jet profiles. The exponential profile agrees with experiments only up to $z/z_{\frac{1}{2}m} \approx 1{\cdot}2$ for the CD region, whereas the free jet profile gives better agreement for both CD and RD regions.

3.4. *Skin-friction behaviour*

Skin friction is usually expressed by its coefficient defined by

$$c_f = \tau_0/(\tfrac{1}{2}\rho U_m^2),$$

where τ_0 is the wall shear stress. In two-dimensional and axisymmetric wall jets, as in the case of boundary layers, the skin-friction variation is expressed as a power law, viz.

$$c_f = K(Re_{y_m})^{-N},$$

where K is a constant of proportionality and $Re_{y_m} = U_m y_m/\nu$.

No direct skin-friction measurements appear to be available in three-dimen-

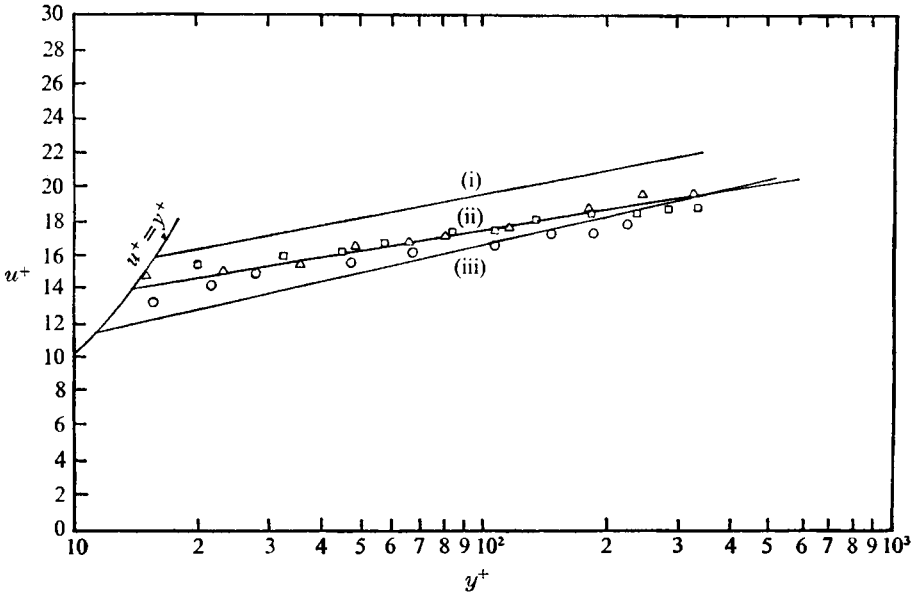

FIGURE 11. Law of the wall at $z = 0$. (i) $u^+ = 4{\cdot}55\log y^+ + 10{\cdot}48$ (Bradshaw & Gee); (ii) $u^+ = 4{\cdot}14\log y^+ + 9{\cdot}1$ (R. P. Patel); (iii) $u^+ = 5{\cdot}5\log y^+ + 5{\cdot}45$ (V. C. Patel). $x/R = 22$ (△), 28 (□), 40 (○).

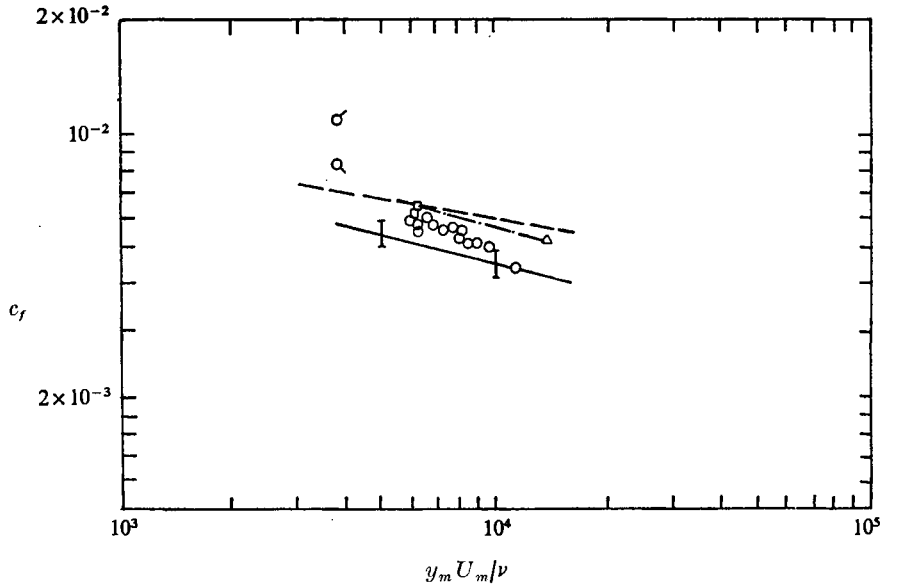

FIGURE 12. Skin-friction distribution in the wall jet. At $z = 0$: ○, present data, $Re_D = 7{\cdot}8\times10^4$; △, calculated from Chandrasekhara Swamy & Lakshmana Gowda, $Re_D = 1{\cdot}18\times10^5$; □, extrapolated from $\widetilde{u'v'}$ measurements. At $z = +75$, -75 mm: ○, ○, from viscous sublayer measurement at $x/R = 34$. ——, Mathieu & Tailland; —·—·—, Sigalla; – – –, Bradshaw & Gee.

sional wall jets. For a wall jet of the present type, Chandrasekhara Swamy & Lakshmana Gowda reported an estimation of skin-friction variation based on Clauser's (1954) method. The jet Reynolds number was $1{\cdot}18 \times 10^5$, and the result was reported as the variation of c_f with distance.

With the velocity profiles as described in § 3.3, it is possible to estimate the skin-friction variation in the plane of symmetry using the method of Clauser, as Chandrasekhara Swamy & Lakshmana Gowda described. This, of course, requires a knowledge of the law of the wall constants for the inner layer of the wall jet. According to Pai & Whitelaw (1969), these constants for wall jets are different from those for boundary-layer or pipe flows. Irwin (1973) showed, by careful measurements, that the constants are the same as those recommended by V. C. Patel (1965), i.e. 5·5 and 5·45. We used the values of 5·75 and 4·9, normally used in boundary-layer literature, to calculate the shear velocity by the Clauser technique, which was then used to convert the data into the U^+ against y^+ form shown in figure 11. It may be seen from figure 11 that our data follow the wall law due to R. P. Patel, as quoted by Pai & Whitelaw (1969), more closely than that of V. C. Patel (1965). A recalculation of shear velocity using the new wall-law constants (viz. 4·14 and 9·1 in the Clauser chart) showed a negligible change in its value, and in those of the wall-law constants.

The skin-friction coefficient distribution in the power-law form is shown in figure 12. For comparison, two-dimensional wall jet results of Bradshaw & Gee (1960), Sigalla (1958) and Mathieu & Tailland (1963) are also shown. It may be seen that our results fall between Sigalla's and Mathieu & Tailland's relations. The scatter is due mostly to different Re_{y_m} values, and is of the same order as that in Mathieu & Tailland's case. Values of c_f from Chandrasekhara Swamy & Lakshmana Gowda have also been shown for extending the Re_{y_m} range. These also have the same trend as the present data. Since Clauser's method is only approximate, Sigalla's relation can be used for all practical purposes up to $Re_{y_m} = 2 \times 10^4$ in the present case.

A check on the order of c_f values was obtained by calculating them from the extrapolated values of the shear-stress distribution (Bandyopadhyay 1974) at $x/R = 38$ and 40 in the plane of symmetry. (The characteristics of turbulent shear stress, especially in relation to the problem of so-called 'energy reversal', have been discussed elsewhere by the authors.) They are also included in figure 12; and they may be seen to agree fairly well with the values obtained by Clauser's method. The figure also contains two c_f values obtained from viscous sublayer measurements, from the same source, at spanwise locations for $x/R = 34$ and $z = 75$ and -75 mm. These values do not follow any of the trends.

4. Turbulence characteristics

4.1. *Axial variation*

The variation of the longitudinal turbulence intensity along the axial direction measured at $y = y_m$ is shown in figure 13, along with the axial variation of the same component with x/D for the 57 mm diameter free jet. (It should be noted that the nozzle exit momentum flux of the free jet is double that of the wall jet.)

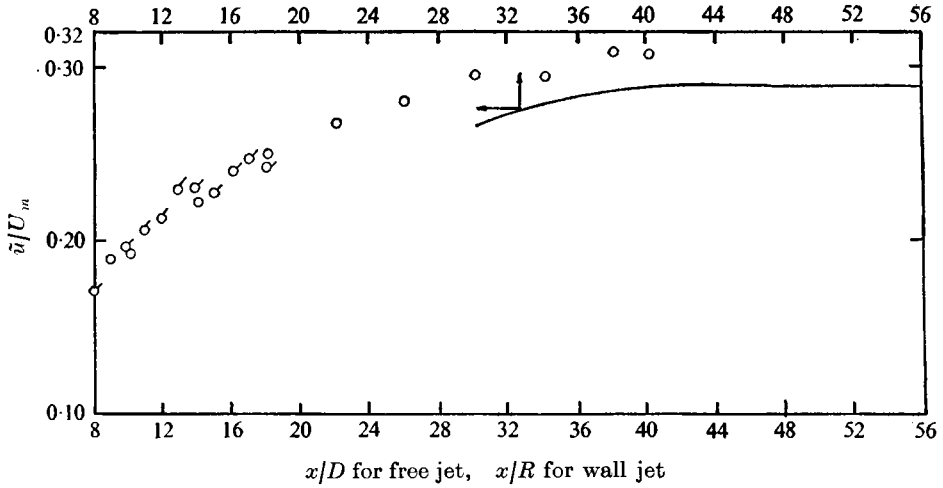

FIGURE 13. Axial variation of longitudinal turbulence intensity at maximum velocity points. ♂, free-jet data (57 mm dia.); ○, wall-jet data. ——, mean curves (Wygnanski & Fiedler's axisymmetric free jet), $\tilde{u}'/U_m$.

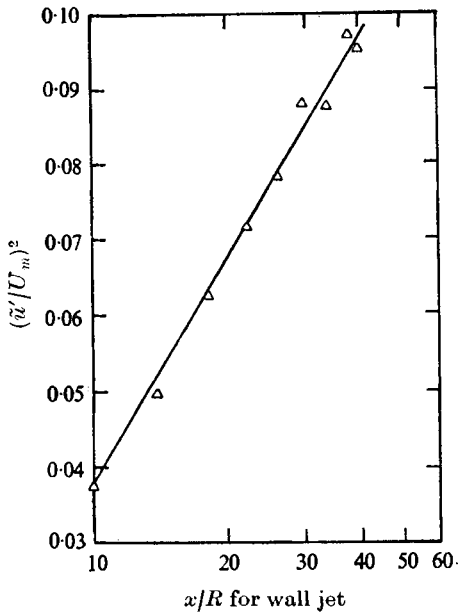

FIGURE 14. Axial variation of $\tilde{u}'$ turbulence in the RD region of the wall jet at $y = y_m$. ——, $(\tilde{u}'/U_m)^2 = 0{\cdot}10\log(x/R) - 0{\cdot}0615$.

The mean curve through Wygnanski & Fiedler's (1969) axisymmetric free jet data is shown for comparison; the intensity for these data becomes constant beyond $x/D = 40$. A similar trend is noticeable for the wall jet data also. But similarity in the turbulent intensity distribution is achieved only after mean velocity profile similarity has been achieved in the RD region beyond $x/R = 22$. Of course, it is to be expected that similarity in the lateral turbulence intensities is possible only much further downstream.

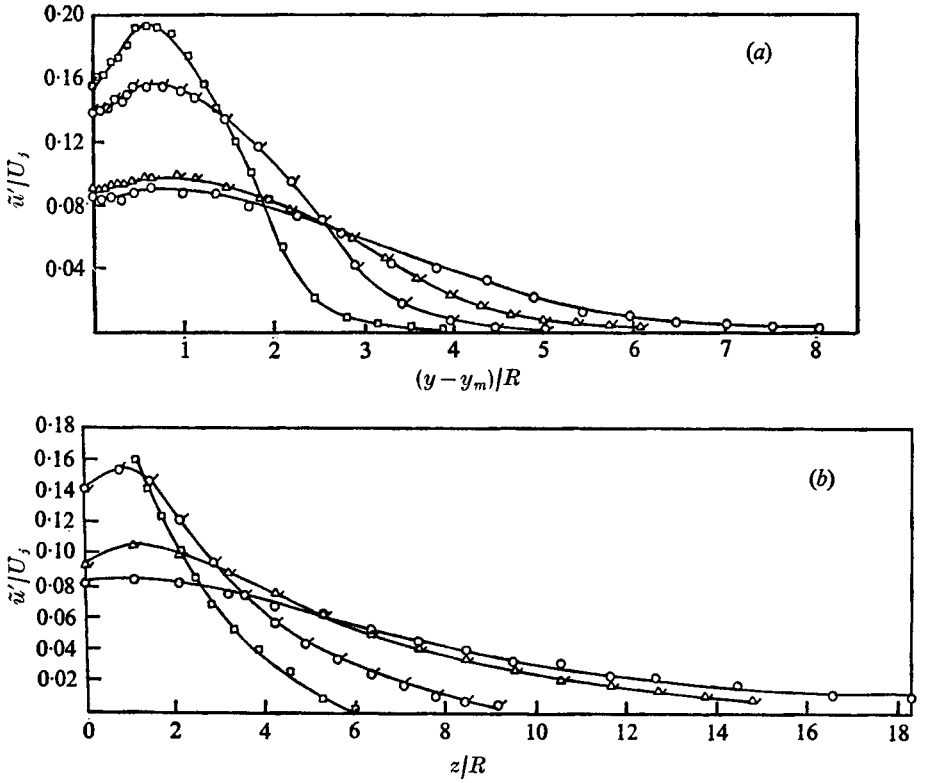

FIGURE 15. Distributions of axial turbulence velocities in (*a*) the outer layer of the wall jet in the plane of symmetry, (*b*) the spanwise direction at $y = y_m$.

x/R	□	○	△	○
(*a*)	10	20	30	40
(*b*)	10	18	30	40

In addition to the above features, for the same axial distance, a wall jet exhibits a higher turbulence level than an axisymmetric free jet. Newman *et al.* noted that the axial turbulence level in a three-dimensional wall jet is about 50 % higher than that for a two-dimensional one, which was also observed in the present case. Simultaneous entrainment of potential fluid in both the y and z directions causes lateral stretching of the eddies in the z direction, which is greater than that in the y direction. Both the higher level of turbulence and the subsequent faster rate of development can be attributed to this. In the y direction, however, the development is slower in the plane of symmetry.

It is possible to describe empirically the axial variation of the longitudinal turbulence at $y = y_m$ in the RD region. This is shown in figure 14. An equation of the form

$$(\tilde{u}'/U_m)^2 = 0{\cdot}10\log(x/R) - 0{\cdot}0615$$

describes the data quite well. One can find a use for this in the closure problem for the RD region of the three-dimensional wall jet, where closure is sought through a model for the distribution of kinetic energy.

The axial turbulence velocities for the outer layer, non-dimensionalized by the

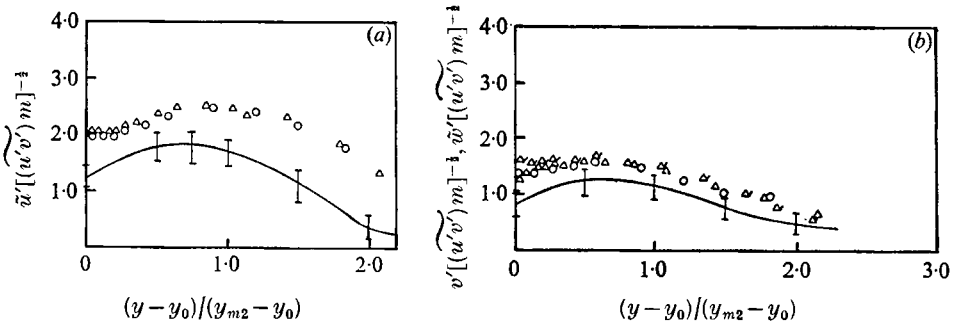

FIGURE 16. Distributions, beyond the point of zero shear stress (i.e. y_0), in the plane of symmetry of the wall jet, of (*a*) $\tilde{u}'$ intensity at $x/R = 36$ (○) and 38 (△), and (*b*) $\tilde{v}'$ and $\tilde{w}'$ intensities at $x/R = 36$ (○, $\tilde{v}[\widetilde{(u'v')}m]^{-\frac{1}{2}}$), 38 (△) and 38 (△, $\tilde{w}'[\widetilde{(u'v')}m]^{-\frac{1}{2}}$).

jet exit velocity, are shown in figure 15 (*a*). The distribution closely resembles a similar plot for an axisymmetric free jet (as reported by Corrsin 1943), indicating the similarity of the turbulence development pattern of the outer layer of the wall jet to that of an axisymmetric free jet. Figure 15 (*b*) shows the turbulence velocity distribution in the spanwise direction at $y = y_m$, for values of x/R of 10, 18, 30 and 40 (i.e. for the CD and the RD regions). Though the result is shown here on only one side of the centre-line, it is closely symmetrical about the centre-line. The distributions in figure 15 (*b*) are similar to those in figure 15 (*a*).

Kruka & Eskinazi (1964), in their studies on wall jets in a moving stream, suggested that non-dimensionalization of $\tilde{u}'^2$ yields meaningful results, when the square root of the maximum shear stress is used as a scaling factor. Correspondingly, the non-dimensionalized length becomes $(y = y_0)/(y_{\frac{1}{2}m} - y_0)$. Figure 16 (*a*) shows the longitudinal turbulence intensity in these co-ordinates, for $x/R = 36$ and 38 and in the plane of symmetry. The mean curve through Kruka & Eskinazi's data is also shown for comparison. There is a tendency towards the turbulence intensity being locally a minimum at $y = y_0$, and the general turbulence level is higher by about 50 %. Figure 16 (*b*) shows the data for the $\tilde{v}'$ and $\tilde{w}'$ intensities, in the same co-ordinates, compared with Kruka & Eskinazi's data. The intensity distributions are close to each other and the intensity levels for the present wall jet are slightly higher. Also, the maximum occurs away from $y = y_0$, closer to y_m. This indicates that the effect of the wall is felt beyond y_m.

The distribution of the three turbulence intensities in the plane of symmetry and at $x/R = 36$ is shown in figure 17 (*a*) for the complete wall jet. The velocity and length scales are respectively U_m and $y_{\frac{1}{2}m}$. This figure shows that, in the outer layer ($y > y_m$), $\tilde{v}'$ and $\tilde{w}'$ are of the same order, but $\tilde{u}'$ exhibits values about 50 % higher. Near the wall ($y < y_m$), the relative distributions are similar to those found in a boundary layer along a smooth wall with zero pressure gradient (Klebanoff 1954). But the levels of all the turbulence components here are much higher than those for a boundary layer. Also, there is no evidence of any isotropy.

The $\tilde{v}'$-turbulence intensity was also measured at $x/R = 34$ and 38, in the plane of symmetry. The distribution of this intensity across the wall jet is shown in figure 17 (*b*) for all the three stations (viz. $x/R = 34$, 36 and 38). The effect of the wall is clearly seen in the fact that, as the wall is approached, the fluctuations

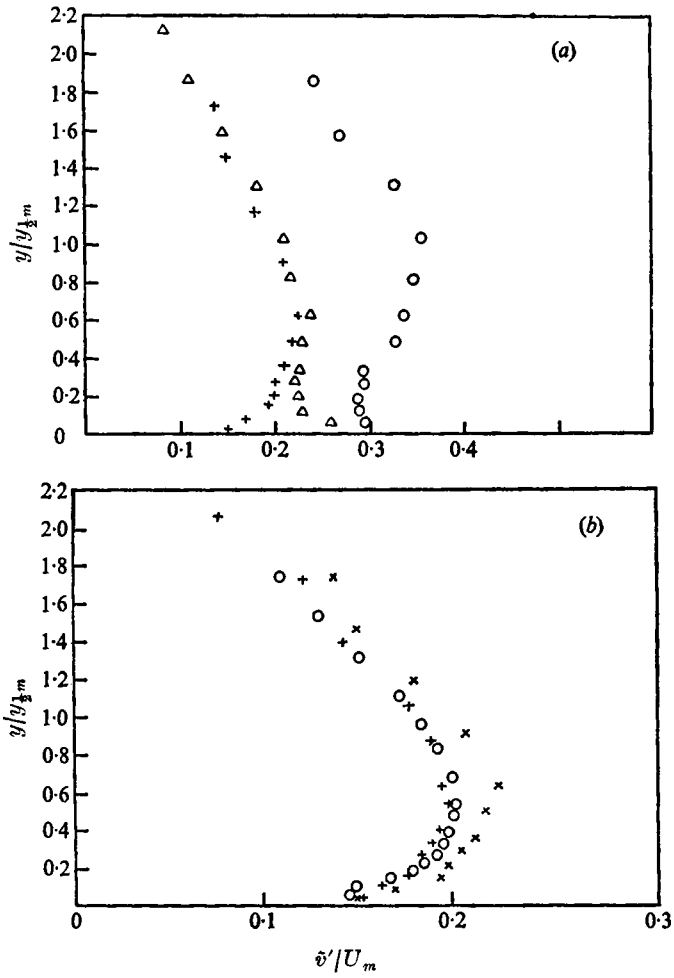

FIGURE 17. (*a*) Comparison of distributions of Reynolds direct stresses at $x/R = 36$ and $z = 0$. ○, $\tilde{u}'/U_m$; +, $\tilde{v}'/U_m$; △, $\tilde{w}'/U_m$. (*b*) Intensity of $\tilde{v}'$ turbulence of the wall jet at $x/R = 34$ (○), 36 (×) and 38 (+).

are more and more damped. Since the three stations are not far from each other, they exhibit nearly the same levels of turbulence.

Since all the Reynolds direct stresses were known in the plane of symmetry at $x/R = 36$, it was possible to find out the distribution of turbulent kinetic energy across the wall jet. The distribution of kinetic energy was found to have roughly the same shape as that of the $\tilde{u}'$ intensity. An approximate estimate for the kinetic energy along the axial direction can be obtained from figure 15 with the assumption that $\tilde{v}'$ and $\tilde{w}'$ are of the same order throughout and bear the same ratio to $\tilde{u}'$ everywhere in the outer layer, as at $x/R = 36$.

4.2. *Spanwise variation*

The longitudinal turbulence intensity distributions in the spanwise direction were measured at a distance from the wall where the maximum velocity occurred (i.e. $y = y_m$), and in both the CD and RD regions. The results for the RD region

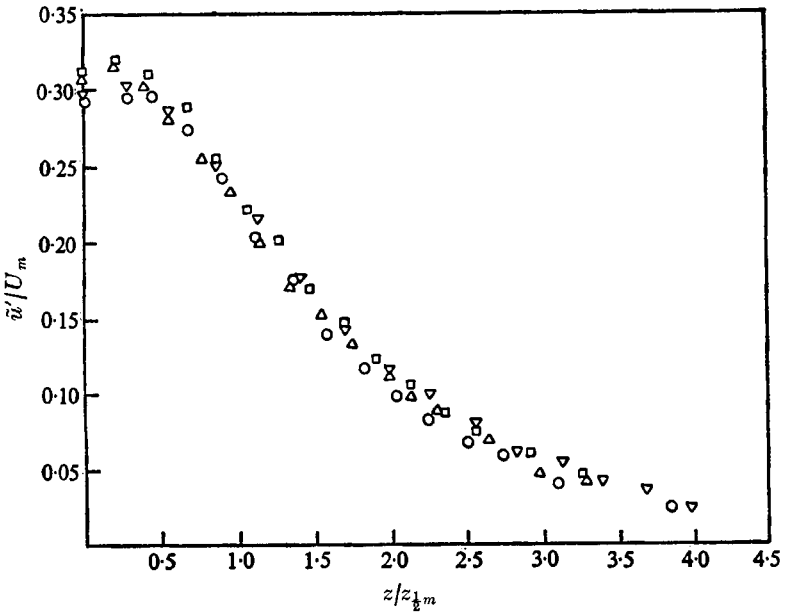

FIGURE 18. Spanwise ($+z$) distribution, at a distance y_m from the wall, of longitudinal turbulence intensities ($\tilde{u}'/U_m$) in the wall jet.

	▽	○	□	△
x/R	30	34	38	40

are shown in figure 18. Barring a tendency for a small local minimum near $z = 0$, the distributions follow a reasonably similar pattern. Such a state is achieved in a free jet only near $x/D = 40$ (Wygnanski & Fiedler 1969). This can be explained by the fact that the wall jet has a spanwise development rate double that of the corresponding free jet. Irwin (1973) reported such behaviour for a plane wall jet with a positive pressure gradient, but at an axial distance of 82·2 times the slot height.

In view of the $\tilde{u}'/U_m$ distribution's following a closely similar pattern, as shown in figure 18, it will be interesting to compare it with the corresponding distribution for an axisymmetric free jet, as given by Wygnanski & Fiedler (1969), especially for $x/D \geqslant 50$. The radial distances for the free jet have been normalized in their case with x. For large x, it matters little whether x is measured from the nozzle face or the virtual origin. In the present case, x is not large enough to be independent of this choice. But, the existence of two virtual origins for the present wall jet makes this choice complicated. For these reasons, the length dimensions of the present data for $x/R = 40$ have been normalized with respect to both R and x, and the result is shown in figure 19. In the case of the z/R representation, barring a small region near $z = 0$, the wall jet data agree fairly well with the axisymmetric free jet data, up to a lateral distance where U/U_m drops to approximately 0·34. Beyond this, the hot-wire measurements must be treated with caution, since the relative intensity of turbulence becomes large.

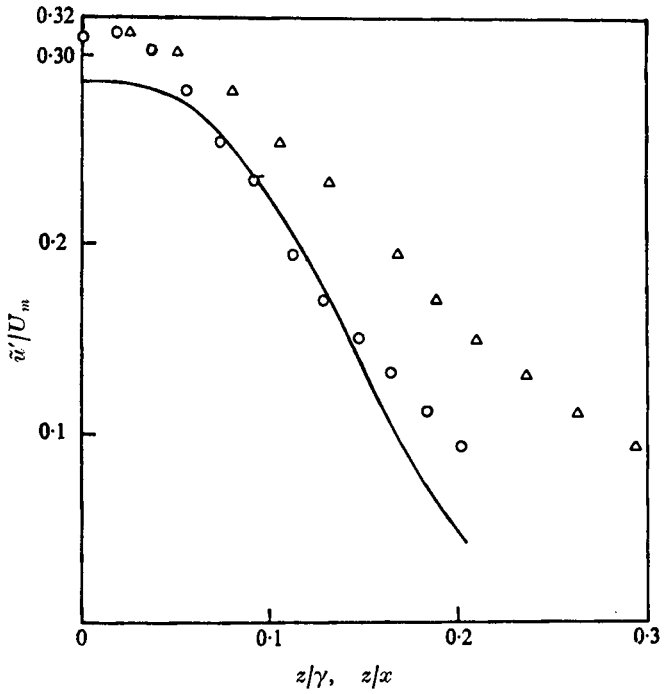

FIGURE 19. Spanwise distribution of the axial turbulence velocity in the wall jet. Location: $x/R = 40$, $r/R = 40 + 17{\cdot}5$, $y = y_m$. ——, mean curve through self-preserving free jet data Wygnanski & Fiedler). ○, z/γ; △, z/x.

5. Concluding remarks

On the basis of the results reported above, several conclusions can be drawn about the behaviour of the three-dimensional wall jet studied here. It is possible to distinguish clearly the existence of the three regions (viz. the potential core, the characteristic decay and the radial-type decay regions). Compared with the case where the orifice is placed flush with the plate, the growth of the wall jet for the present geometry is faster, since a larger area of contact between the free jet and the wall is available for the wall friction to influence the wall jet growth. An important characteristic, noticed by other investigators also, is that the growth rate of the wall jet in the spanwise direction is larger than that in the axial direction. The different rates of spread in the two directions give rise to two virtual origins. The virtual origin for the axial growth is upstream of the orifice face, which is also the case with axisymmetric free jets. But the virtual origin for the spanwise growth is downstream of the orifice face. The existence of two virtual origins, so widely separated from each other (approximately 25 radii), makes the flow complicated. It would, of course, be interesting to study what influence the geometry of the jet has on the relative locations of the virtual origins. For instance in the case of the orifice flush with the plate (Newman *et al.* 1972), the relative displacement is of the order of 36 jet diameters.

The estimation of skin friction in wall jets by the Clauser technique appears to give results quite close to those cited by others. Even though there is no general agreement on the wall-law constants for a wall jet, it is possible to choose

representative values for them that yield reliable estimates for the skin friction.

The turbulence level in a three-dimensional wall jet is generally higher than that for corresponding two-dimensional wall jets and free jets. This is significant in those flow situations where good mixing is desired within a short distance from the nozzle. The spanwise axial turbulence distribution at the point of maximum velocity approaches a self-similar form for the present geometry at a rate faster than that for the axisymmetric free jet. This is possibly due to the larger spanwise spread of the flow field, as mentioned earlier. The area of contact between the free jet and the wall is maximum when the wall is placed in a diametral plane. It can thus be speculated that the present geometry gives a development rate of the wall jet faster than that due to any other position of the wall relative to the nozzle. Naturally, this needs confirmation by further experiments.

The authors are grateful to Prof. B. S. Murthy and Mr V. Ganesan of the Internal Combustion Engines Laboratory of I.I.T., Madras, for making available to them some of the experimental facilities.

REFERENCES

BANDYOPADHYAY, P. 1974 Some studies on a developing three-dimensional incompressible turbulent wall jet. Ph.D. thesis, I.I.T., Madras.

BRADSHAW, P. & GEE, M. T. 1960 *Aero. Res, Counc. R. & M.* no. 3252.

CHANDRASEKHARA SWAMY, N. V. & LAKSHMANA GOWDA, N. H. 1974 *Z. Flugwiss.* **22**, 314.

CLAUSER, F. H. 1954 *J. Aero. Sci.* **21**, 91.

CORRSIN, S. 1943 *N.A.C.A. Wartime Rep.* W94.

DAVIES, P. O. A. L., FISHER, M. J. & BARRATT, M. J. 1963 *J. Fluid Mech.* **15**, 337.

GLAUERT, M. B. 1956 *J. Fluid Mech.* **1**, 625.

HANJALIĆ, K. & LAUNDER, B. E. 1972 *J. Fluid Mech.* **52**, 609.

HINZE, J. O. 1959 *Turbulence.* McGraw-Hill.

IRWIN, H. P. A. H. 1973 *J. Fluid Mech.* **61**, 33.

KLEBANOFF, P. S. 1954 *N.A.C.A. Tech. Note*, no. 3178.

KRUKA, V. & ESKINAZI, S. 1964 *J. Fluid Mech.* **20**, 555.

LAWN, C. J. 1969 *CEGB RD Rep.* B/M 1277.

MATHIEU, J. & TAILLAND, A. 1963 *C. R. Acad. Sci.* **256**, 2768.

NEWMAN, B. G., PATEL, R. P., SAVAGE, B. S. & TJIO, H. K. 1972 *Aero. Quart.* **23**, 188.

PAI, B. R. & WHITELAW, J. H. 1969 *Aero. Quart.* **20**, 355.

PATANKAR, V. P. & SRIDHAR, K. 1972 *J. Basic Engng*, **94**, 339.

PATEL, V. C. 1965 *J. Fluid Mech.* **23**, 185.

POREH, M., TSUEI, Y. G. & CERMAK, J. E. 1967 *J. Appl. Mech.* **34**, 459.

SCHLICHTING, H. 1968 *Boundary Layer Theory*, 6th edn. McGraw-Hill.

SCHWARZ, W. H. & COSART, W. P. 1961 *J. Fluid Mech.* **10**, 481.

SFORZA, P. M. & HERBST, G. 1970 *A.I.A.A. J.* **8**, 276.

SHAW, R. 1960 *J. Fluid Mech.* **7**, 550.

SIGALLA, A. 1958 *J. Roy. Aero. Soc.* **62**, 873.

SRIDHAR, K. & TU, P. K. C. 1966 *J. Roy. Aero. Soc.* **70**, 669.

VIETS, H. & SFORZA, P. M. 1966 *Dept. Aero. Engng, App. Mech, Poly. Inst. Brooklyn Rep.* PIBAL 968.

WYGNANSKI, I. & FIEDLER, H. 1969 *J. Fluid Mech.* **38**, 577.